An Measurement of Deeply Virtual Compton Scattering with Transversely Polarized Neutron using the SoLID Spectrometer

A new letter of intent to Jefferson Lab PAC43

Alexandre Camsonne[1], Haiyan Gao[2], Carlos Muñoz Camacho[3], Gu Chao[4], Kondo Gnanvo[4], Nilanga Liyanage[4], Marie Boer[3], Zhihong Ye[2], Zhiwen Zhao[2], and and the Hall A SoLID collaboration[1]

[1] Thomas Jefferson National Accelerator Facility
[2] Duke University
[3] Institut de Physique Nucleaire Orsay
[4] University of Virginia

May 12, 2015

Abstract

We propose to perform, for the first time at JLab, the asymmetry measurements of the deeply virtual Compton scattering (DVCS) with transversely-polarized neutrons using the new solenodial large acceptance device (SoLID) in Hall-A. The spin azimuthal dependence of the asymmetries in various kinematic regions can be used to constrain the distributions of Compton form factors (CFFs), which correspond to the integrals of Generalized Parton Distributions (GPDs). The high luminosity and large acceptance features of the SoLID will provide precise information of the neutron GPDs, in particular the GPD E^n which has not been well studied but crucial for the study of J_u and J_d in the Ji's sum rule via a flavor decomposition. We plan to use exact the same setup as the approved SIDIS experiments, but with a minimum modification of adding the photon-detection trigger.

Contents

1 Introduction

In the last 50 years, the experimental exploration of the nucleon structure with electron accelerators has been mainly focused on two classes: measurements of form factors (FFs) through the elastic scattering to obtain the information about the spatial density of nucleons; and measurements of the inclusive deep inelastic process to obtain the parton distribution functions (PDFs) which contain the nucleon's momentum density. Using various experimental techniques, a large group of data with great precision and extensive coverage has provided powerful inputs to understand the mechanism of the hadron structure, and meanwhile, revealed many unsolved puzzles.

In 1990s, a new concept for the description of the nucleon structure was introduced by Mueller, Ji and Radyushkin [1–4], known as the Generalized Parton Distributions (GPDs). GPDs provide a link between electromagnetic form factors and parton distributions [5, 6] within the same formalism. What's more, they probe the internal dynamics of the nucleon, e.g. the transverse spatial distribution as a function of the longitudinal momentum fraction of the quarks. One of the important applications is to quantify the angular momentum of quarks contributed to the nucleon spin through the Ji's sum rule [2].

Deeply Virtual Compton Scattering (DVCS) is the golden channel to experimentally study GPDs [6]. In electron scattering off nucleons with sufficient large momentum transfer, one measures the hard exclusive photons produced in the Bethe-Heitler (BH) and the DVCS processes as well as their interference, and isolates the DVCS amplitude which is described in terms of GPDs.

Several DVCS experiments with proton targets have been carried out in Hall A and Hall B at Jefferson with 6 GeV electron beam. The Hall A experiment [14, 27] focused on the precise helicity-dependent and helicity-independent cross section measurements in a limited phase-space. The Hall B experiment used CLAS [15,28] to measure the beam-spin and target-spin asymmetries and cross sections over a large kinematic range with limited precision. Meanwhile, the HERMES experiments have measured various asymmetries [17–24] using 27 GeV electron and positron beams on unpolarized, longitudinally polarized and transversely polarized proton targets, but their results suffer from large uncertainties. With the 12 GeV upgrade, several experiments in Hall A and B using CLAS12 have been approved to measure the beam-spin asymmetry and target-spin asymmetry with longitudinally polarized proton target [9, 10].

The DVCS measurement on neutrons is more difficult mainly due to less production yields, smaller asymmetries and bigger demands on the experimental techniques compared with the proton-DVCS case. The first neutron-DVCS measurement was performed in the E03-106 experiment in Hall A with polarized beam on a deuterium target. This pioneering work established the importance of the neutron-DVCS measurement but was limited to a narrow phase space. An approved CLAS12 experiment [11] aims to measure the beam-spin asymmetry with unpolarized neutron target. To allow for a fully flavor decomposition to extract the GPDs of individual quarks, it is desired to collect precise neutron data in a more complete phase space and with more experimental observables, especially with the transversely polarized target which is essential to access the GPD E. The main goal of this proposal is to perform the first measurement of the DVCS on transversely polarized neutrons with 11 GeV longitudinally polarized electron beam.

2 Motivation

2.1 Generalized Parton Distributions

The DVCS amplitude can be factorized into two parts in the Bjorken limit: the hard scattering part which can be precisely calculated by perturbative QCD, and the soft part which contains information about the electromagnetic structure of the nucleon, described by a list of Generalized Parton Distributions (GPDs), H, E, $\tilde{H}$ and $\tilde{E}$, where the first two functions, called unpolarized GPDs, correspond with averages of the quark/gluon helicity, and the last two functions involve differences of quark/gluon helicities and hence are called polarized GPDs. In the rest of this proposal, unless specified, we will only discuss the GPDs of quarks in the valence region.

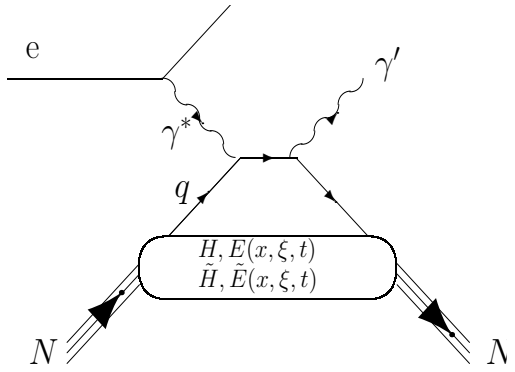

Figure 1: Handbag diagram of the DVCS process

As shown in Fig. 1, a highly virtual photon scatters on a quark of which the initial and final momentum fractions are given as $x+\xi$ and $x-\xi$, respectively. The struck quark goes back to its initial nucleon by emitting a real photon so the nucleon remains intact. GPDs are functions of x, ξ and t, where x denotes the average light-cone momentum fraction of the quark and is not experimentally measurable; ξ represents the longitudinal momentum fraction transferred to the nucleon and in Bjorken limit of infinite Q^2, it reduces to $\xi = x_{bj}/(2-x_{bj})$, where x_{bj} is the well known DIS variable defined as $x_{bj} = Q^2/(2k\cdot k')$ where k and k' are the initial and final four momenta of the electron; t represents the total square momentum transferred to the nucleon, given as $t = \Delta^2 = (p-p')^2$, where p and p' are the four momenta of the nucleon before and after the scattering, respectively. The GPDs also depend on Q^2 but the variation can be predicted through the evolution equations and doesn't reveal the non-perturbative part of the nucleon. In practice, the Q^2 dependence is usually dropped out from the expressions.

The elastic form factors can be given by the first moments of the GPDs [7]:

$$\int_{-1}^{+1} dx H^q(x,\xi,t) = F_1^q(t), \tag{1}$$

$$\int_{-1}^{+1} dx E^q(x,\xi,t) = F_2^q(t), \tag{2}$$

$$\int_{-1}^{+1} dx \tilde{H}^q(x,\xi,t) = G_A^q(t), \tag{3}$$

$$\int_{-1}^{+1} dx \tilde{E}^q(x,\xi,t) = G_p^q(t), \tag{4}$$

where q denotes the quark flavor. $F_1^q(t)$ and $F_2^q(t)$ are the Dirac and Pauli form factors, g_A^q and g_P^q are the axial and pseudoscaler form factors, respectively. The GPDs H, $\tilde{H}$ are linked to the parton distribution functions, $q(x)$ and $\Delta q(x)$ in the forward limit:

$$H^q(x,\xi=0,t=0) = q(x), \tag{5}$$

$$\tilde{H}^q(x,\xi=0,t=0) = \Delta q(x), \tag{6}$$

One of the most important properties of the GPDs is the Ji's sum rule which would give access to the contribution of quark angular momentum to the nucleon's spin:

$$J^q = \frac{1}{2}\Delta\Sigma^q + L^q = \frac{1}{2}\int_{-1}^{+1} dx x[H^q(x,\xi,t=0) + E^q(x,\xi,t=0)], \tag{7}$$

where $\Delta\Sigma^q$ is the contribution of the spin of quarks which was already measured in polarized deep inelastic scattering. Note that the sum rule also applies to the gluon GPDs. Hence the Ji's sum rule provides an experimental way to decompose the nucleon spin in terms of the quark and gluon contributions. Together with measurements of the quark spin in the DIS process, the sum rule will determine the quark orbital angular momentum contribution to the nucleon spin.

In order to study the contribution of the quark orbital angular momentum (L_q) to the nucleon spin, one needs to determine the E and H GPDs for each quark. However, experimentally, we only measure the GPDs of neutron and proton instead of quarks. Similar to the determination of FFs and PDFs of different quarks, one has to measure both the neutron and proton GPDs and then carry out a flavor separation. For example, in the valance quark region,

$$H^p(\xi,\xi,t) = \frac{4}{9}H^u(\xi,\xi,t) + \frac{1}{9}H^d(\xi,\xi,t), \tag{8}$$

$$H^n(\xi,\xi,t) = \frac{1}{9}H^u(\xi,\xi,t) + \frac{4}{9}H^d(\xi,\xi,t), \tag{9}$$

form which obtains:

$$H^u(\xi,\xi,t) = \frac{9}{15}(4H^p(\xi,\xi,t) - H^n(\xi,\xi,t)), \tag{10}$$

$$H^d(\xi,\xi,t) = \frac{9}{15}(4H^n(\xi,\xi,t) - H^p(\xi,\xi,t)). \tag{11}$$

The same relation holds for $\tilde{H}$, E and $\tilde{E}$.

2.2 Deeply Virtual Compton Scattering

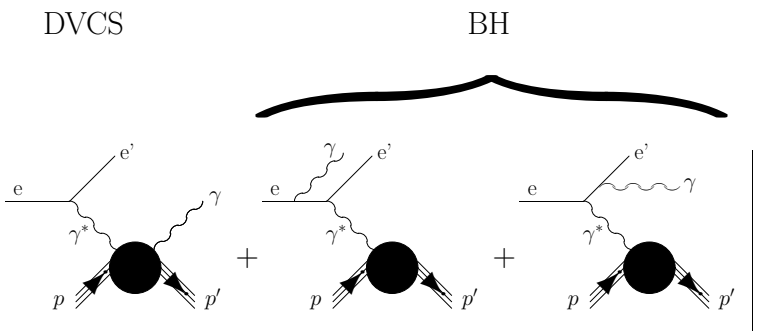

Figure 2: DVCS and Bether-Heitler processes in the $e + N \to eN\gamma$ reaction. The cross section is composed of the amplitudes of these two processes as well as their interference term.

The $e + N \to eN\gamma$ reaction is composed of two processes including the DVCS and the Bethe-Heitler (BH) processes. The later one describes the radiation of the photon by the incoming or scattered electron, as shown in Fig. 2. The measure differential cross section of the hard exclusive photon production can be given as the sum of the DVCS, BH processes and their inference:

$$\frac{d^5\sigma}{dx_{bj}dydtd\phi d\varphi} = \frac{\alpha^3 x_{bj} y}{16\pi^2 Q^2\sqrt{1+\varepsilon^2}}|\mathcal{T}|^2 \tag{12}$$

where $\varepsilon = 2x_{bj}M/Q$ and y is the fraction of the electron energy lost in the nucleon rest frame. As shown in Fig. 3, ϕ is the angle between the leptonic plane and the hadronic plane and φ is the angle between the polarization vector and the recoil nucleon. The reaction amplitude, $|\mathcal{T}|^2$, can generically be expressed as:

$$|\mathcal{T}|^2 = |\mathcal{T}_{DVCS}|^2 + |\mathcal{T}_{BH}|^2 + \mathcal{I}, \tag{13}$$

$$\mathcal{I} = \mathcal{T}^*_{DVCS}\mathcal{T}_{BH} + \mathcal{T}^*_{BH}\mathcal{T}_{DVCS}, \tag{14}$$

where $\mathcal{T}_{DVCS}$ and $\mathcal{T}_{BH}$ represent the amplitudes of the DVCS and BH processes, and $\mathcal{I}$ denotes their inference term. Fig. 3 illustrates the $e + N \to eN\gamma$ reaction with relevant kinematic variables.

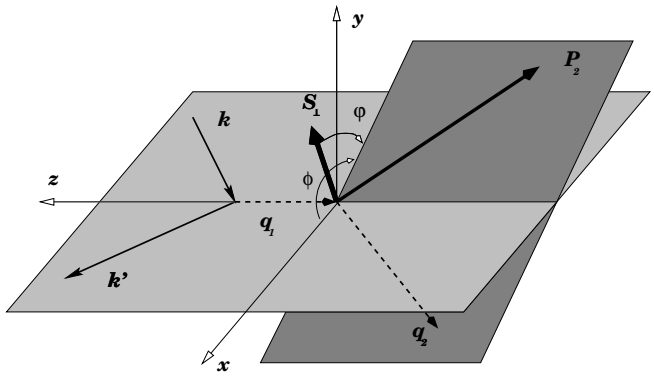

Figure 3: Reference frame of the DVCS process. The reference frame is composed of two planes: the directions of the incoming electron and the scattered electron form the leptonic plane. The directions of the recoil nucleon and the real photon in the final state form the hadronic plane. This plot shows the target in the transversely polarized case where the x and y directions are in and perpendicular to the leptonic plane, respectively.

The DVCS amplitude contains the information about the GPDs with the convolution integral:

$$\mathcal{T}_{DVCS} \propto \int_{-1}^{+1} dx \frac{H(x,\xi,t)}{x-\xi+i\epsilon} = \mathcal{P}\int_{-1}^{+1} dx \frac{H(x,\xi,t)}{x-\xi} - i\pi H(\xi,\xi,t), \tag{15}$$

where $\mathcal{P}$ denotes the principal value integral. Eq. (15) can be decomposed into a real and an imaginary part, and including other GPDs E, $\tilde{H}$ or $\tilde{E}$, there are eight GPD-related quantities that can be extracted from the DVCS process [7]:

$$H_{Re}(\xi,t) \equiv \mathcal{P}\int_0^1 dx \left[H(x,\xi,t) - H(-x,\xi,t)\right] C^+(x,\xi), \tag{16}$$

$$H_{Im}(\xi,t) \equiv H(\xi,\xi,t) - H(-\xi,\xi,t), \tag{17}$$

$$E_{Re}(\xi,t) \equiv \mathcal{P}\int_0^1 dx \left[E(x,\xi,t) - E(-x,\xi,t)\right] C^+(x,\xi), \tag{18}$$

$$E_{Im}(\xi,t) \equiv E(\xi,\xi,t) - E(-\xi,\xi,t), \tag{19}$$

$$\tilde{H}_{Re}(\xi,t) \equiv \mathcal{P}\int_0^1 dx \left[\tilde{H}(x,\xi,t) + \tilde{H}(-x,\xi,t)\right] C^-(x,\xi), \tag{20}$$

$$\tilde{H}_{Im}(\xi,t) \equiv \tilde{H}(\xi,\xi,t) + \tilde{H}(-\xi,\xi,t), \tag{21}$$

$$\tilde{E}_{Re}(\xi,t) \equiv \mathcal{P}\int_0^1 dx \left[\tilde{E}(x,\xi,t) + \tilde{E}(-x,\xi,t)\right] C^-(x,\xi), \tag{22}$$

$$\tilde{E}_{Im}(\xi,t) \equiv \tilde{E}(\xi,\xi,t) + \tilde{E}(-\xi,\xi,t), \tag{23}$$

with the coefficient functions $C^{\pm}$ defined as :

$$C^{\pm}(x,\xi) = \frac{1}{x-\xi} \pm \frac{1}{x+\xi} \tag{24}$$

Note that one has reduced the x-range of integration from $\{-1,1\}$ to $\{0,1\}$ in the convolutions. Eq. 16 through Eq. 23 are refer to as the Compton form factors (CFFs). For convenience, four complex functions are introduced:

$$\begin{aligned}
\mathcal{H}(\xi,t) &\equiv H_{Re}(\xi,t) - i\pi H_{Im}(\xi,t), &(25)\\
\tilde{\mathcal{H}}(\xi,t) &\equiv \tilde{H}_{Re}(\xi,t) - i\pi \tilde{H}_{Im}(\xi,t), &(26)\\
\mathcal{E}(\xi,t) &\equiv E_{Re}(\xi,t) - i\pi E_{Im}(\xi,t), &(27)\\
\tilde{\mathcal{E}}(\xi,t) &\equiv \tilde{E}_{Re}(\xi,t) - i\pi \tilde{E}_{Im}(\xi,t). &(28)
\end{aligned}$$

On the other hand, the BH amplitude can be precisely calculated theoretically with the well measured F_1 and F_2 form factors. The BH cross section strongly depends on the kinematic variables, Q^2, x_{bj}, t or ϕ. One of the distinct features is a sharply enhancement around $\phi = 0$ or $\phi = 180$ which corresponds to the regions where the radiated photon is along the directions of the incoming electron or the scattered one, respectively. The BH amplitude varies significantly over the entire phase space and it can be either overwhelming or can be ignored when compared with the DVCS amplitude. One can look for unique experimental observables that are sensitive to the $\mathcal{I}$ term, such that the linear combination of CFFs can be directly accessed via the DVCS amplitude while the BH amplitude thereupon serves as an asset.

2.3 Experimental Observable

Taking into account the fact that the four GPDs reflect different combination of the nucleon spin and quark helicities, one is sensitive to different combinations of them by measuring various experimental quantities with different beam and target polarization. For example, one can measure DVCS with different beam- and/or target-spin polarizations as the cross section differences give access to the interference term ($\mathcal{I}$) of the BH and DVCS processes [7, 8]:

$$\begin{aligned}
\Delta\sigma_{LU} &\propto \sin\phi \;\; Im\{F_1\mathcal{H} + \xi(F_1+F_2)\tilde{\mathcal{H}} - kF_2\mathcal{E} + ...\}, &(29)\\
\Delta\sigma_{UL} &\propto \sin\phi \;\; Im\left\{F_1\tilde{\mathcal{H}} + \xi(F_1+F_2)\left(\tilde{\mathcal{H}} + \frac{x_{bj}}{2}\mathcal{E}\right) - \xi k F_2\tilde{\mathcal{E}} + ...\right\}, &(30)\\
\Delta\sigma_{LL} &\propto (A + B\cos\phi) \;\; Re\left\{F_1\tilde{\mathcal{H}} + \xi(F_1+F_2)\left(\mathcal{H} + \frac{x_{bj}}{2}\mathcal{E}\right) + ...\right\}, &(31)\\
\Delta\sigma_{UTx} &\propto \sin\phi \;\; Im\{k(F_2\mathcal{H} - F_1\mathcal{E}) + ...\}, &(32)\\
\Delta\sigma_{LTx} &\propto (A + B\cos\phi) \;\; Re\left\{k(F_2\mathcal{H} - F_1\mathcal{E}) + ...\right\}, &(33)
\end{aligned}$$

where $\Delta\sigma$ stands for a cross section difference at certain beam (first subscript) and target (second subscript) polarization directions ("U" for unpolarized, "L" for longitudinally polarized, and "Tx" or "Ty" for transversely polarized in (x) or perpendicular (y) to the leptonic plane as shown in Fig. 3). Furthermore, F_1 and F_2 are the Dirac and Pauli form factors, and the kinematic variable k is defined as : $k = -t/(4m_N^2)$. The detailed correlations between the cross sections and the DVCS+BH amplitudes have been worked out in Ref. [8].

From Eq. 29 to Eq. 33, each cross section difference is only sensitive to certain CFFs when neglecting terms multiplied by kinematic factors with small values, such as ξ, x_B or k. For example, among these proton CFFs, $Im\{\mathcal{H}^p\}$ dominates in $\Delta\sigma_{LU}$ and instead, $Im\{\tilde{\mathcal{H}}^p\}$ is the largest contribution to $\Delta\sigma_{UL}$. One also notices that the observables with single-spin polarization access the imagine parts of the CFFs while the double-spin polarization terms probe the real parts. The sensitivity of these observables to the neutron CFFs changes due to different FFs values, e.g. $F_1^n \approx 0$ when t is small.

During the experiments it is simpler to measure the asymmetries with various beam and target polarization to avoid the normalization issue, even though the sensitivity to the CFFs is not as direct as the one from the cross section difference.

3 Proposed Measurements-Transversely Polarized Neutron DVCS

We propose to measure spin azimuthal asymmetries in deep virtual Compton scattering on transversely polarized neutrons by using a new Solenoidal Large Intensity Device (SoLID) in Hall A. Both the scattered

electron and the real photon will be measured coincidentally after the longitudinally polarized incoming electron with $E_{beam} = 8.8\ GeV$ or 11 GeV scattering off the ^{3}He target. The beam single spin asymmetry (BSA), the target single spin asymmetry (TSA) and the double spin asymmetry (DSA) will be extracted from the data and their azimuthal dependence can give access to both real and imaginary parts of corresponding Compton Form Factors (CFFs). The transversely polarized neutron data is particularly sensitive to the GPD E^n which is hard to be measured and least known. Combined with other GPDs, H^n, H^p and E^p, one can perform a flavor decomposition to extract the GPDs for u and d quarks, and investigate the contribution of quark orbital angular momenta to the nucleon spin using the Ji's sum rule.

The measurement will be carried out with exactly the same configuration as the one used in the approved experiment, E12-10-006 [26], which will measure the semi-inclusive deep inelastic scattering process. The SoLID is able to handle a very high luminosity (up to $10^{36} cm^{-2} s^{-1}$), and also has a large acceptance ($0.8 \leq P \leq 7.5\ GeV/c$, $8^\circ \leq \theta \leq 24^\circ$, and $0^\circ \leq \phi \leq 360^\circ$). Such nice features enable us to perform the measurement with high precision and extensive kinematic coverage. An introduction of the experimental setup will be given in next section.

We plan to perform a multi-dimensional binning on the new data and the results will provide strong constraints on the values of CFFs. An analysis technique [7] to extract the CFFs with asymmetry data has been successfully employed in the data analysis of the 6 GeV experiments in Hall A [14] and in Hall B with CLAS [15], as well as the HERMES experiments [17–24], assuming a leading twist formalism. A new CLAS12 experiment, C12-12-010, was proposed in Hall B to perform the similar measurement but with a transversely polarized proton target (i.e., HDICE), and was conditionally approved because of an on-going effort of developing the new HDICE target.

4 Experimental setup

In the current SoLID design [25], there are two configurations dedicated to the parity violation deep inelastic scattering (PVDIS) experiments and the semi-inclusive deep inelastic scattering experiments (SIDIS). We will use the same detector system as the approved SIDIS experiments, E12-10-006, E12-11-007, and E12-11-108, but with a minimum modification of the trigger design to include photon detection. In this section, we will briefly introduce the polarized ^{3}He target and the SoLID detector system in the SIDIS configuration. A discussion of additional requirements for the new measurement will be also given and followed by a description of the conceptual trigger design.

4.1 Transversely Polarized ^{3}He Target

Target	^{3}He
Length	40 cm
Target Polarization	$\sim$60%
Target Spin Flip	$\leq$20 mins
Target Dilution	90%
Effective Neutron	86.5%
Target Polarimetry Accuracy	$\sim$ 3%

Table 1: Key Parameters of the ^{3}He target.

The proposed measurement will utilize the same polarized ^{3}He as E12-10-006 [26]. Such a target was successfully employed in E06-110, a 6 GeV SIDIS experiment in Hall A. The polarization direction is held by three sets of Helmholtz coils with a 25 Gauss magnetic filed. Both the transverse and longitudinal directions can be provided by rotating the magnetic field. The ^{3}He gas with density of about 10 atm (at 0°) is stored in a 40 cm target cell made of thin glasses. With a 15 μA electron beam, the neutron luminosity can be as high as $10^{36} cm^{-2} s^{-1}$. The in-beam polarization of 60% was archived during the E06-110 experiment. Two kinds of polarimetry, NMR and EPR, were used to measure the polarization with relative 5% precision. We have planed to improve the accuracy of the measurement to reach 3%.

The target spin will be reversed for every 20 minutes by using the RF AFP technique. The additional polarization loss due to the spin reversal was kept at < 10 % which has been taken into account in the overall 60% in-beam polarization. A new method for spin reversal using filed rotation has been tested and was able to eliminate the polarization loss. Such an improvement will enable us to perform the spin-reversal in few minutes to reduce the target-spin-correlated systematics. The key parameters of the ^{3}He target are summarized in Table 1.

A collimator, similar to the one used in the E06-110, will be placed next to the target cell window to minimize the target cell contamination and to reduce the event rate. Several calibration targets will also be installed in this target system, including a multi-foil ^{12}C for optics study, a BeO target for beam tunning, and a reference target cell for dilution study and other calibration purposes.

4.2 SoLID Spectrometer and Detectors

The solenoid magnet for SoLID will be based on the CLEO-II magnet built by Cornell University. The magnet is 3 meters long with the out diameter of 3 meters and the inner diameter of 1 meter. The field strength is greater than 1.35 Tesla with integrated BDL of 5 Tesla-meters. The fringe filed at the front end after shielding is less than 5 Gauss. In the SIDIS-configuration, the CLEO-II magnet provides 2π acceptance in the azimuthal angle (ϕ) and covers the polar angle (θ) from 8° up to 24°. The momentum acceptance is between 0.8 and 7.5 GeV/c and the resolution is about 2%.

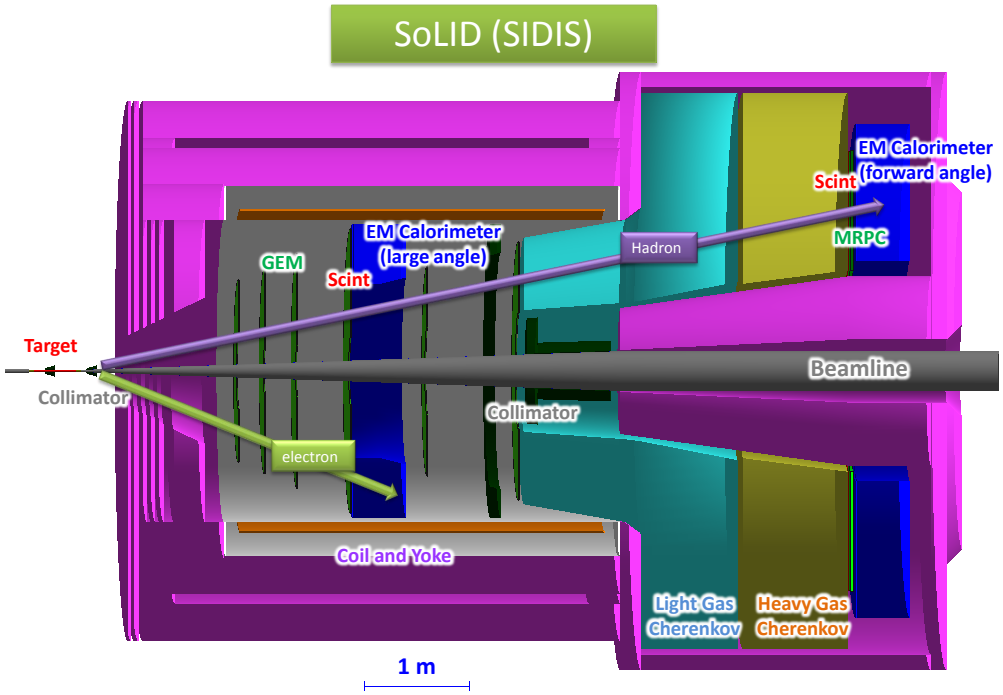

Figure 4: The Detector Layout of the SoLID-SIDIS configuration. The detector system includes six Gas Electron Multiplier (GEM) planes for charged particle tracking, two Scintillator Pad Detectors (SPD) followed by two Shashlyk sampling EM Calorimeters (EC) for energy measurement and particle identification, a Light Gas Čerenkov Detector (LGC) for e-$\pi^{\pm}$ separation, a Heavy Gas Čerenkov Detector (HGC) for $\pi^{\pm}$-$K^{\pm}$ separation, as well as a Multi-gap Resistive Plate Chamber (MRPC) for timing measurement. The first four GEM trackers, the first SPD (i.e. LASPD) and EC (i.e. LAEC) form the large-angle detection system for electron measurement. The forward-angle detection system, to measure electron and hadrons, is composed of all six GEM trackers, LGC, HGC, MRPC, the second SPD (i.e. FASPD) and the second EC (FAEC). The photon-detection in the large-angle is given by the veto-signal of the SPD in coincidence with the EC signal, where the photons in the forward-angle system will be triggered by the EC signal plus the veto-signals of LGC, SPD, and MRPC.

The layout of the SoLID detectors in the SIDIS-configuration is shown in Fig. 4. The detector system

Experiments	SIDIS	DVCS
Reaction channel	$(e, e'\pi^{\pm})$	$(e, e'\gamma)$
Target	^{3}He	^{3}He
Unpolarized luminosity	$\sim 10^{37}$ cm^{-2}s^{-1}	$\sim 10^{37}$cm^{-2}s^{-1}
Momentum coverage (GeV/c)	0.8-7.5	0.8-7.5
Momentum resolution	$\sim$2%	$\sim$2%
Polar angle coverage	8°-24°	8°-24°
Polar angle resolution	0.6 mr	0.6 mr
Azimuthal angle resolution	5 mr	5 mr
Target Vertex resolution	0.5 cm	0.5 cm
Energy resolution on ECs	5%$\sim$10%	$\leq$5%
Position resolution on ECs	1 cm on x and y	$\leq$1 cm on x and y
Trigger type	Coincidence $e^- + \pi^{\pm}$	Coincidence $e^- + \gamma$
Expected DAQ rates	<100 kHz	<100 kHz
Backgrounds	(e,$\pi^-\pi^{\pm}$) (e,e'K$^{\pm}$)	$(e, e'\pi^0)$
Major requirements	Radiation hardness DAQ Kaon Rejection	Radiation hardness DAQ Pion Rejection Energy resolution

Table 2: Summary of Key Parameters for DVCS Measurement compared with SIDIS Experiments.

is divided into two parts for the forward-angle detection and the large-angle detection. Six Gas Electron Multiplier (GEM) tracking chambers will be used for charged particle tracking, where only four of them will be used for the large-angle detection. In each part, a Shashlyk-type sampling EM calorimeter (LAEC or FAEC) will measure the particle energy and identify electrons from hadrons, while a scintillator-pad detector (LASPD and FASPD) will be installed in front of each EC to reject photons. The forward-angle detectors will detect both the electrons and hadrons (mainly $\pi^{\pm}$). A light-gas Čerenkov detector (LGC) and a heavy-gas Čerenkov detector (HGC) will perform the $e/\pi^{\pm}$ and $\pi^{\pm}/K^{\pm}$ separation, respectively. The Multi-gas Resistive Plate Chamber (MRPC) will provide a precise timing measurement and serve as a backup of the FASPD on photon rejection.

A more detailed discussion of the design, simulation, prototype-test of each detector is given in the SoLID preliminary conceptual design report (pCDR) [25].

4.3 Additional Requirements for DVCS Measurement

To use the existing SIDIS configuration for the DVCS measurement, it requires few minimum modifications. Both the scattered electrons and the photon will be detected to form the coincidence trigger. The photon-detection is not included in this configuration but can be easily added. In principle, the new measurement may be carried out along with the E12-10-006 by simply adding the photon trigger in addition to the electron and hadron triggers. New beam time will be requested in the actual proposal if more statistics are required to reach the proposed precision, or there are additional commissioning and calibration tasks needed, and last but not the least, the modification of the existing experimental configuration will bring significant impact to the SIDIS measurements.

Since the recoil neutrons will not be detected, we will need to reconstruct the neutron missing mass spectrum to make sure the exclusivity of the measurement. On top of the similar hardware requirements as the SIDIS experiments, the DVCS measurement has greater demand on the detector resolutions. For electrons, the GEM tracking reconstruction is able to achieve very good accuracy on determining the momentum ($\sim$2%) and the angles ($\sim 0.6\ mrad$ on θ_e and $\sim 5.0\ mrad$ on ϕ_e). On the other hand, the precision of the photon measurement, however, have to rely on the performance of the ECs. The photon's angular resolutions are determined by the position resolutions of the EC cluster reconstruction, as well as the vertex resolution on the target which is given by the tracking reconstruction of electrons. The current design goal

is to reach $\sim 1.0\ cm$ precision on both the x- and y- directions on the EC plane. The cluster reconstruction will also determine the photon energy resolution within the range of $5\% \sim 10\ \%$. Based on the experience from the Hall A DVCS experiments, a minimum requirement of the energy resolution for photon-detection should be less than $5\%/\sqrt{E}$. To perform the DVCS measurement, it is desired to improve the photon's energy resolution by optimizing both the EC design and the cluster reconstruction.

Furthermore, the DVCS measurement will suffer from a large contamination by the $e + n \rightarrow e + n' + \pi^0$ reaction since a π^0 decays into two photons and the $n' + \gamma$ system mixes in the neutron spectrum. We plan to detect the two-photon events within the acceptance and remove the reconstructed π^0 background. The current EC and DAQ designs should be able to identify two-photon events but further investigation of the performance is required.

Table 2 summarizes the key parameters of the detector system in the SIDIS configuration for both the SIDIS and DVCS measurements.

4.4 Trigger Design

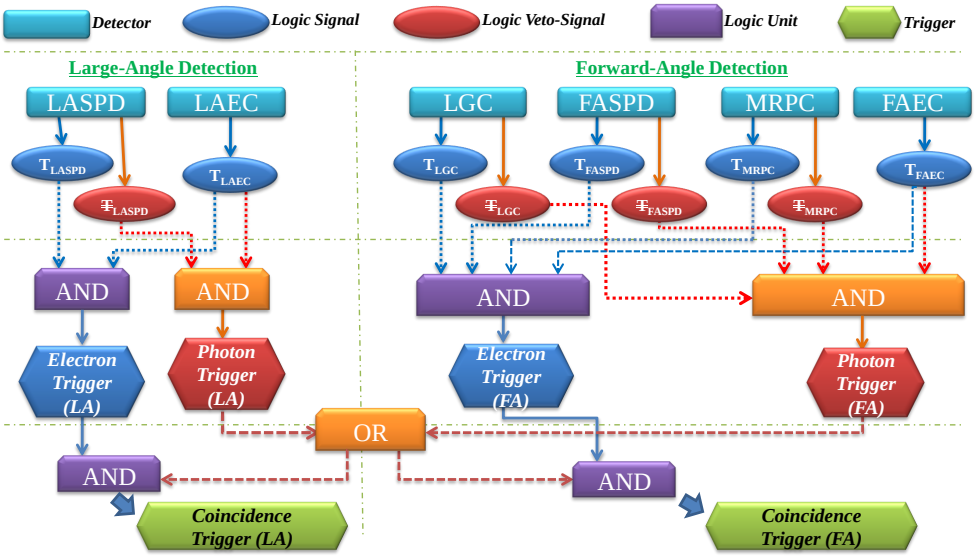

Figure 5: A sketch map of the DVCS trigger design. At the large-angle part (LA), the electron trigger is formed by the "AND" of the LAEC signal and the LASPD signal, while the photon trigger is the coincidence signal of the LAEC signal and the veto-signal from the LASPD. Similarly, at the forward-angle part (FA), the electron trigger is the "AND" of the LGC, FASPD, MRPC and FAEC, and the photon trigger comes from the FAEC signal in coincident with the veto-signals of all other three detectors. Two coincidence signals are formed in the end to provide the event triggers from LA and FA.

The DVCS events will be recorded with the coincidence trigger of the scattered electron and the photon. Both the large-angle detectors and forward-angle detectors can detect these particles at the same time, so two coincidence triggers will be created and sent to the DAQ system. In principle, the DVCS triggers will be similar to the SIDIS trigger, but only the hadron triggers will be replaced by the photon triggers. If the new experiment runs together with E12-10-006, we will simply add two more triggers types on top of the existing SIDIS triggers. Fig. 5 shows a sketch map, in a simplified way, to compose the electron and photon single-triggers, and the coincidence triggers. The actual trigger design will be far more complicated, and the detailed discussion of the trigger and DAQ design has been given in the SoLID pCDR [25].

5 Projection of the Measurement

5.1 Kinematic Coverage

Fig. 6 shows the acceptance of the momenta and polar angles for electrons and photons which are from the DVCS process and can be simultaneously detected in SoLID. The kinematic coverage of the DVCS events within the SoLID acceptance are given in Fig. 7 for the beam energy of 8.8 GeV and 11 GeV. These distributions were weighted by the cross sections calculated with the VGG model [12] and the spectrometer acceptance obtained from the GEANT4 simulation with the SIDIS configuration. As shown in these plots, the range of Q^2 is from 1.0 GeV^2 to 8.0 GeV^2, x_B goes from 0.1 up to 0.75, and t up to -2.0 GeV^2. The distribution for neutrons is also given in Fig. 6. As we can see, almost 80% of neutrons locate at $> 40°$ with very low momenta around 0.4 GeV/c. It is difficult to design a dedicated detector to measure these neutrons. In our proposed measurement, we will not detect the neutron events but only rely on the reconstructed missing mass to perform the DVCS event selection.

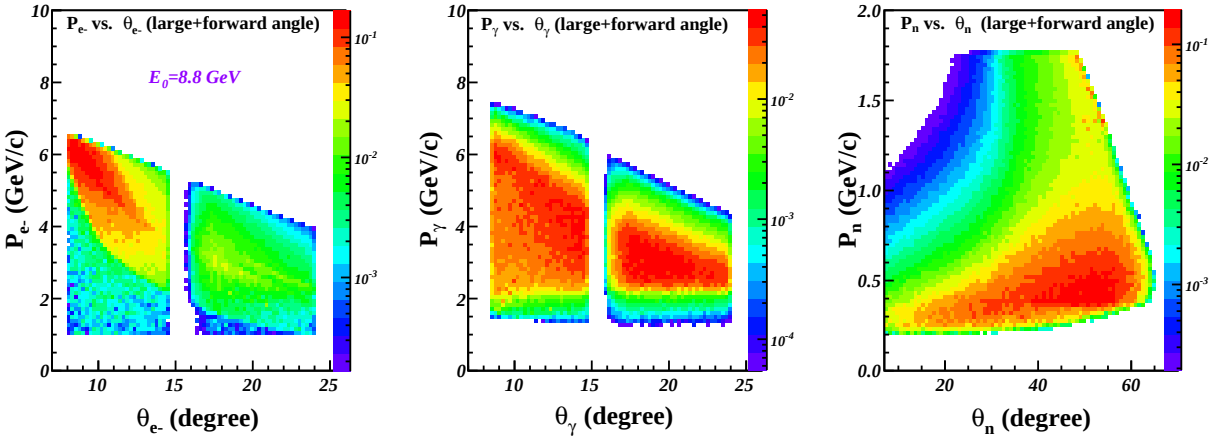

(a) E_{beam}=8.8 GeV

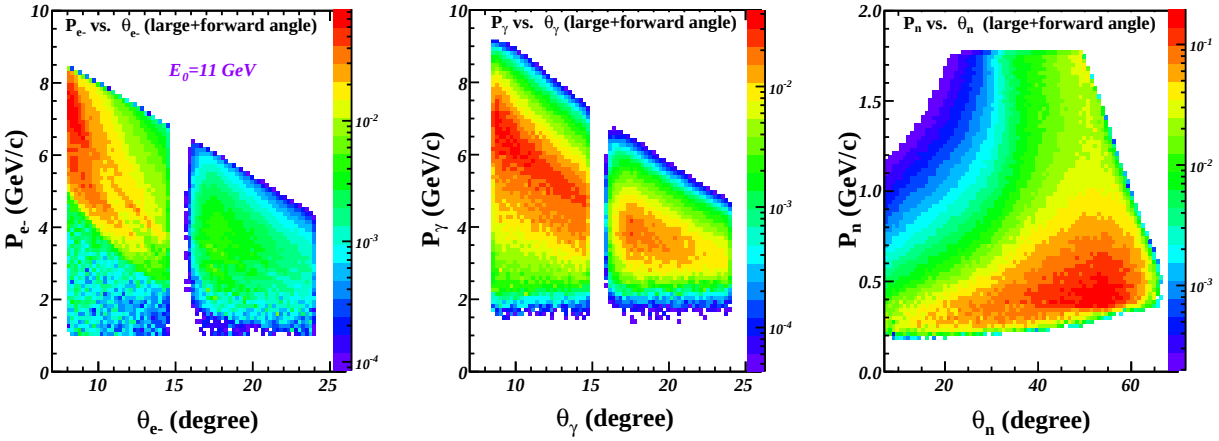

(b) E_{beam}=11 GeV

Figure 6: The acceptance of the momenta and polar angles at E_{beam} = 8.8 GeV (a) and 11 GeV (b) for electrons (left) and photons (mid). The distribution of the undetected neutrons is also given in the right plot as a demonstration. Colors correspond to rates (Hz) in log scale.

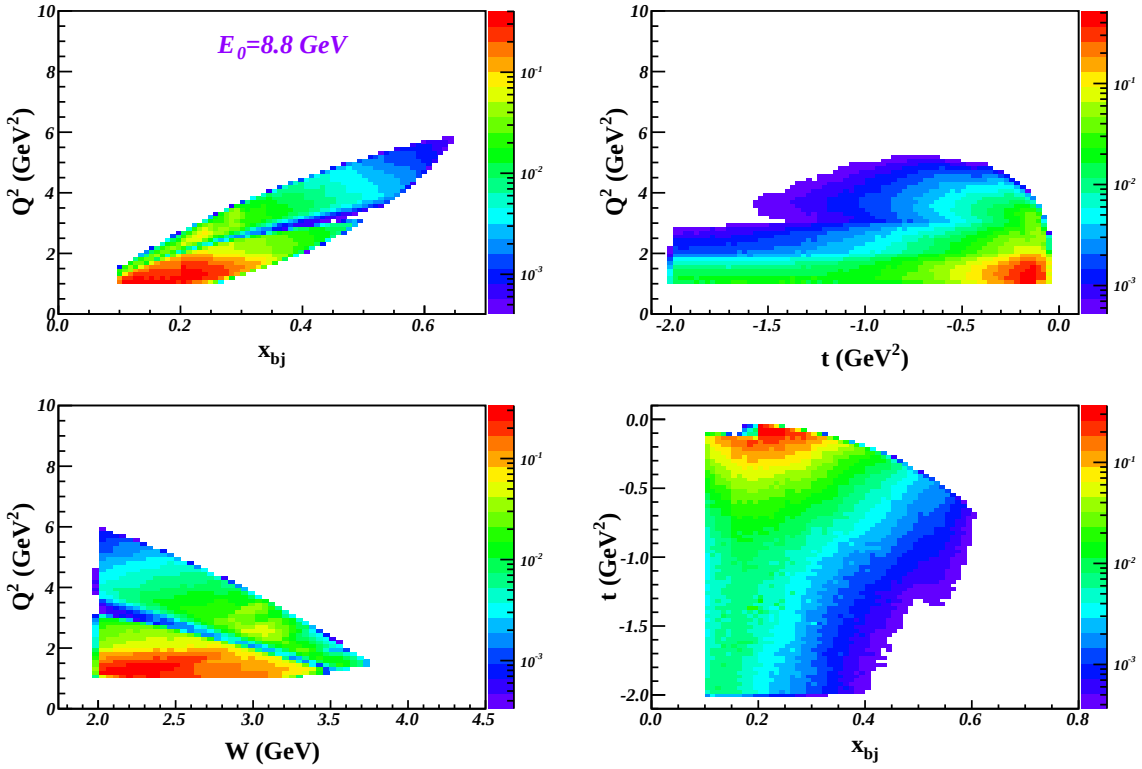

(a) E_{beam}=8.8 GeV

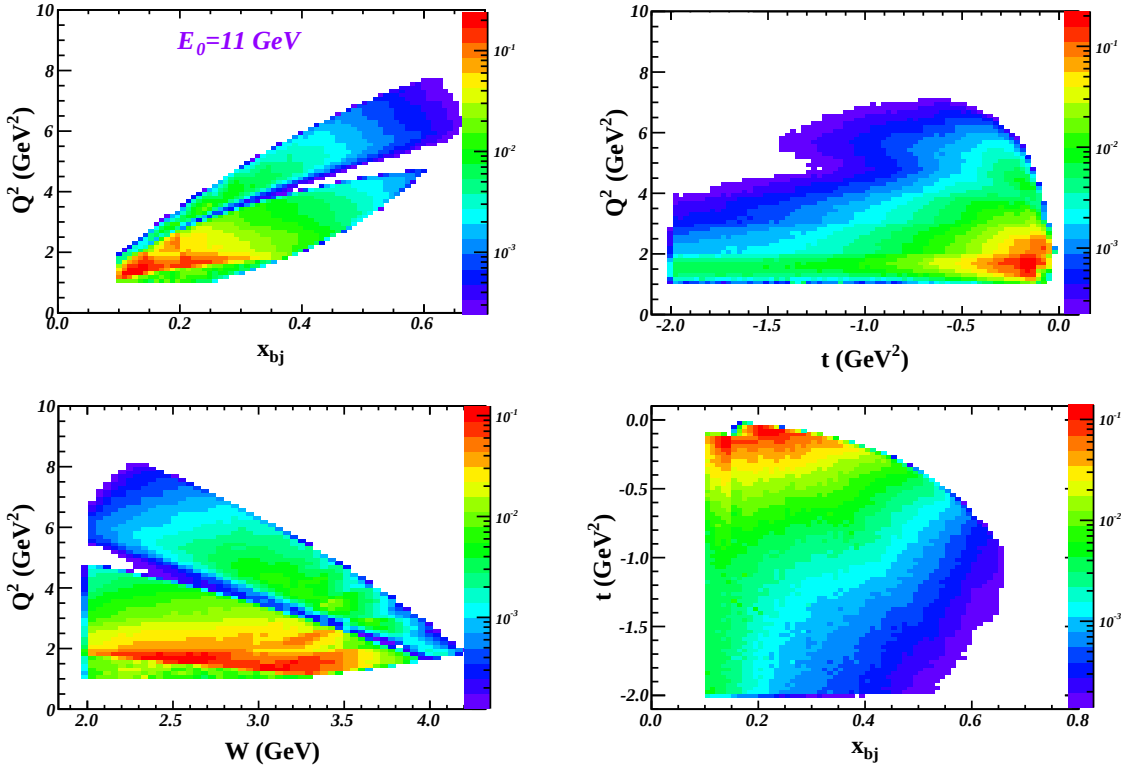

(b) E_{beam}=11 GeV

Figure 7: The coverage of important physics variables at $E_{beam} = 8.8\ GeV$ (a) and 11 GeV (b). Colors correspond to rates (Hz) in log scale.

5.2 Estimated Rates

Table 3 lists the single electron and photon rates at the forward-angle and the large-angle, and the coincidence rate. The rates were calculated with the simulated events weighted by the target luminosity, the SoLID acceptances and cross sections. The electron beam energy at 8.8 GeV and 11.0 GeV are both calculated, respectively. The rates are the unpolarized event rates and are not corrected by the beam and target polarization, target dilution and so on. The total integrated physics rates are estimated to be around 38 Hz at 8.8 GeV and 22 Hz at 11 GeV, respectively.

E_0	8.8 GeV	11 GeV
Single Rates (Hz)		
e- (FAEC)	64.78	36.17
e- (LAEC)	2.57	1.70
γ (FAEC)	45.37	40.54
γ (LAEC)	31.05	28.83
Coincidence Rates (Hz)		
e-(FAEC)+γ(FAEC+LAEC)	36.06	20.50
e-(LAEC)+γ(FAEC+LAEC)	1.46	1.00

Table 3: Integrated rates for neutron-DVCS with transversely polarized ^{3}He. The values are estimated based on cross sections predicted by the VGG model, the SoLID-SIDIS acceptance and the target luminosity.

5.3 Asymmetry Projections

To obtain a preliminary projection of the measurement, we currently assume the proposed experiment will share the beam time with the E12-10-006 which was approved to have 21 days at $E_0 = 8.8\ GeV$ and 48 days at $E_0 = 11\ GeV$. A more detailed beam-time estimation and possible additional beam-time request will be given in the actual proposal. The binning was performed for each target polarization setting (LTx or LTy) but with the combination of data at both energy settings. The simulated data was binned in 4-dimensions with a sequence of Q^2 (5 bins), x_B (5 bins), t (6 bins) and ϕ (12 bins), where the bin size for each variable is determined by the array given as following:

$$Q^2[6] = \{1.0, 1.5, 2.0, 3.0, 4.5, 7.0\}, \quad (5\ bins) \tag{34}$$

$$x_B[6] = \{0.1, 0.2, 0.3, 0.4, 0.5, 0.7\}, \quad (5\ bins) \tag{35}$$

$$t[7] = \{-2.0, -0.7, -0.5, -0.4, -0.3, -0.2, -0.1\}, \quad (6\ bins) \tag{36}$$

$$\phi[13] = \{0, 30, 60, 90, 120, 150, 180, 210, 240, 270, 300, 330, 360\}, \quad (12\ bins). \tag{37}$$

The number of events (N) in each bin is calculated with the total simulated events after applying cuts on the corresponding ranges of these 4 variables. As shown in Eq. 38, each event in one bin is then corrected by the weight of the cross section and the acceptance value of the electron and the photon. N is further normalized by the phase-space (PSF), total generated events (N_{gen}), beam-time ($T_{8.8(11GeV)}$), the target luminosity ($L = 10^{36} cm^{-2} s^{-1}$), and the overall detector efficiency (ϵ_{eff}):

$$N = (\sum_{i \in bin} \sigma_i^{avg} \cdot A_i^{e+\gamma}) \cdot (PSF/N_{gen}) \cdot T_{8.8(11GeV)} \cdot L \cdot \epsilon_{eff}, \tag{38}$$

where $\sigma_i^{avg} = (\sigma_i^{+\uparrow} + \sigma_i^{+\downarrow} + \sigma_i^{-\uparrow} + \sigma_i^{-\downarrow})/4$, is the average of the four cross sections in different beam and target polarization directions ($\pm$ represents the beam polarization and $\uparrow\downarrow$ denotes the target polarization). $A_i^{e+\gamma}$ is the product of the electron and photon acceptance weights for this event. The detector efficiency, ϵ_{eff}, is fixed at 85%.

For four different combinations of the beam and spin polarization directions, their numbers of events in one bin were evaluated and given as $N^{+\uparrow}$, $N^{+\downarrow}$, $N^{-\uparrow}$, and $N^{-\downarrow}$. One can obtain the beam-spin asymmetry

(A_{BS}), target-spin asymmetry (A_{TS}) and double-spin asymmetry (A_{DS}) written as:

$$A_{BS} = \frac{N^+ - N^-}{N^+ + N^-} \frac{1}{P_e} \tag{39}$$

$$A_{TS} = \frac{N^\uparrow - N^\downarrow}{N^\uparrow + N^\downarrow} \frac{1}{f P_T P_n}, \tag{40}$$

$$A_{DS} = \frac{(N^{+\uparrow} + N^{-\downarrow}) - (N^{+\downarrow} + N^{-\uparrow})}{N^{+\uparrow} + N^{+\downarrow} + N^{-\uparrow} + N^{-\downarrow}} \frac{1}{f P_T P_n P_e}, \tag{41}$$

where P_e (beam polarization) and P_T (target polarization) are set to be 90% and 60%, respectively. The dilution factor, f, is chosen to be 90% based on the experience from the E06-110 data analysis, and P_n, the effective polarization of neutrons inside ^{3}He, is known to be about 86.5%.

The absolute statistical uncertainty of the asymmetries are approximately given as:

$$\delta A_{BS} = \frac{1}{\sqrt{N}} \frac{\sqrt{1 - (P_e A_{BS})^2}}{P_e}, \tag{42}$$

$$\delta A_{TS} = \frac{1}{\sqrt{N}} \frac{\sqrt{1 - (f P_T P_n A_{BS})^2}}{f P_T P_n}, \tag{43}$$

$$\delta A_{DS} = \frac{1}{\sqrt{N}} \frac{\sqrt{1 - (f P_T P_n P_e A_{BS})^2}}{f P_T P_n P_e} \tag{44}$$

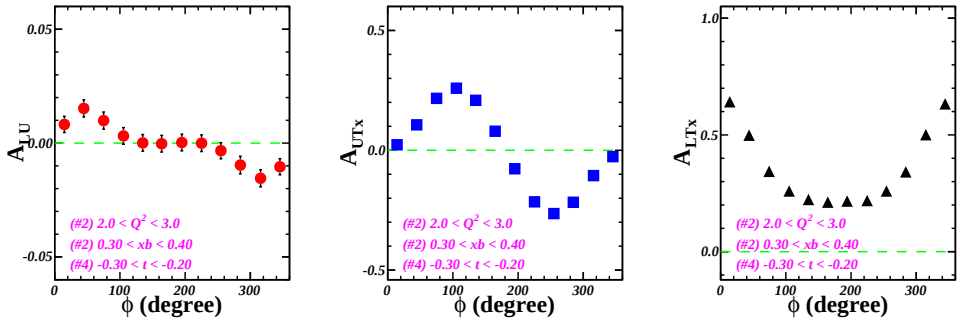

(a) Tx Polarization

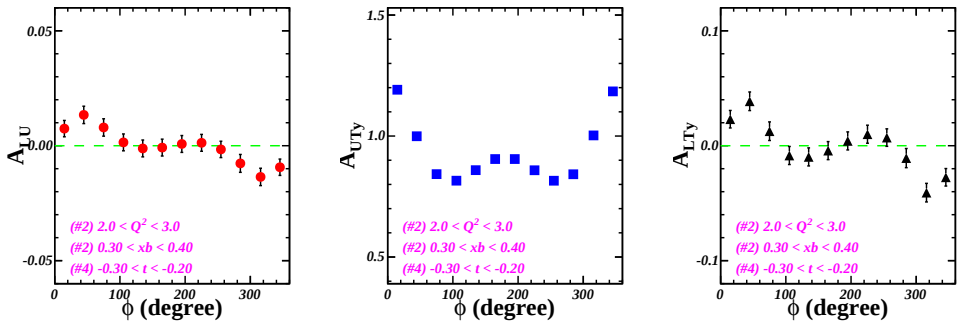

(b) Ty Polarization

Figure 8: Asymmetry distributions with transversely polarized target at one typical bin,$< Q^2 > \sim 2.4\ GeV^2$, $< x_B > \sim 0.35$ and $< t > \sim -0.25$. The plots from left to right give A_{LU}, A_{UTy} and A_{LTy} as functions of ϕ, respectively. Data includes both the $E_{beam} = 8.8\ GeV$ and 11 GeV settings.

The full binning results are given in Appendix A. As an example, the zoom-in plots for one particular (Q^2, x_B, $-t$) setting are given in Fig. 8. In general, the SoLID spectrometer provides extensive coverage and great statistics.

6 Missing Mass and Background

To make sure the exclusivity of the reaction, we need to reject the background events from other processes, such as the $e+n \to e+n'+\pi^0$ channel which is the major background source. In the new measurement, we will only detect scattered electrons and real photons from the DVCS reaction, and reconstruct the neutron missing mass to select the real DVCS events. The π^0 events will be mixed into the missing mass spectrum with the neutron mass plus the energy of one of two photons from π^0 decay. One typical way to remove the background is to apply a cut on the upstream tail of the spectrum and further subtract the residual by fitting the π^0 tail that extends to the neutron spectrum. Such a method relies on good resolutions of the final particle detection and efficient π^0 reconstruction and fitting algorithms.

The momentum (or energy) and angular resolutions for electron measurement are determined by the GEM tracking reconstruction which is designed to achieve the following values:

$$\delta P_e/P_e \sim 2\%, \delta\theta_e \sim 0.6\ mrad, \delta\phi_e \sim 5\ mrad,$$

The resolutions of photon detection are determined by the cluster reconstruction of ECs (including FAEC and LAEC). The energy resolution is about $\sim$ 5% in our current design. The angular resolutions are determined by the EC position resolutions and the target vertex position (δz_{vertex}) given by the electron tracking reconstruction, which are:

$$\delta x_{EC} = 1\ cm, \delta y_{EC} = 1\ cm, \delta z_{vertex} = 0.5\ cm. \tag{45}$$

Since distances between the target to the LAEC and FAEC are 310 m and 790 m, respectively, the angular spreads of photons based the position resolutions in Eq. 45 are about 1.2 $mrad$ on θ and 4.5 $mrad$ on ϕ. We noticed that the energy resolution is the dominant source of the uncertainty when comparing the change of the missing mass resolution by varying the photon's energy and angular resolutions.

With the resolutions of detecting electrons and photons discussed above, we reconstructed the neutron missing mass spectrum, shown in Fig. 9. The Fermi motion of the neutron inside the nucleus was also considered but the effect is negligible compared with the detector resolutions. Due to lack of a model to predict the $e+n \to e+n'+\pi^0$ cross sections, we mixed the π^0 events only with a uniform distribution and scaled the relative amplitude compared with the DVCS events to match the preliminary results from the most recent Hall A DVCS data. The plots given here are served as a demonstration of the missing mass resolution with the current design of the SoLID detectors. With higher beam energy, the π^0 events tend to move further away from the DVCS peak, which makes the current estimation close to the realistic situation. From these two spectra, we noticed that the ability of detecting two photons will help us to suppress nearly half of the π^0 background. Meanwhile, the background tail mixed into the neutron peak is not significant and can be subtracted by fitting the background distribution. We believe that the background can be well controlled with the existing setup, but we are still evaluating the background situation and also plan to improve the detector resolutions. We are working with the Hall A DVCS collaboration to extract the π^0 events from their new data and will develop a phenomenological model to study the background. We will present a more realistic background study in the actual proposal.

The other major source of background will be single-photon production which can affect the online trigger rates but will be easily subtracted during the offline analysis. These events are produced when the electron beam passes through target material (e.g. Bremsstrahlung radiation), or through the secondary scattering when particles interact with the spectrometer, detectors and other materials along the trajectory. In the former case photons travel nearly along the very forward direction ($< 4^\circ$) which is out of the SoLID acceptance. Photons in the later case usually carry very low energy and based on the background study of the SoLID-SIDIS experiment, a $\geq 1\ GeV$ threshold setting on the photon trigger is sufficient to remove these background. One can increase the threshold during the experiment if the rate is still high since the main photon events are above 2 GeV, as shown in Fig. 6. Residual single photon events can be removed during the offline analysis by cutting on the missing mass spectrum. We expect that this type of background can be well controlled.

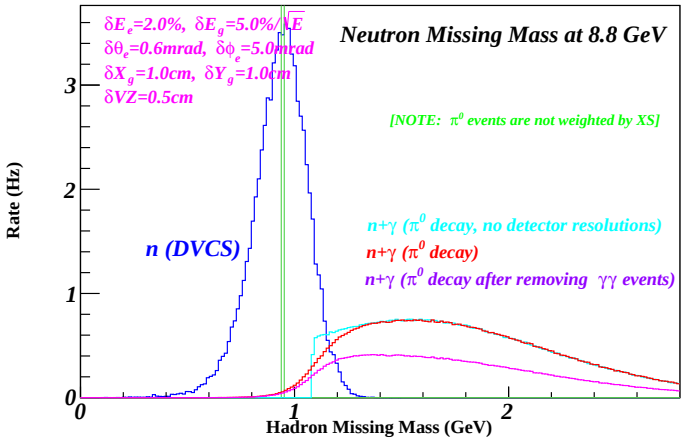

(a) E_{beam}=8.8 GeV

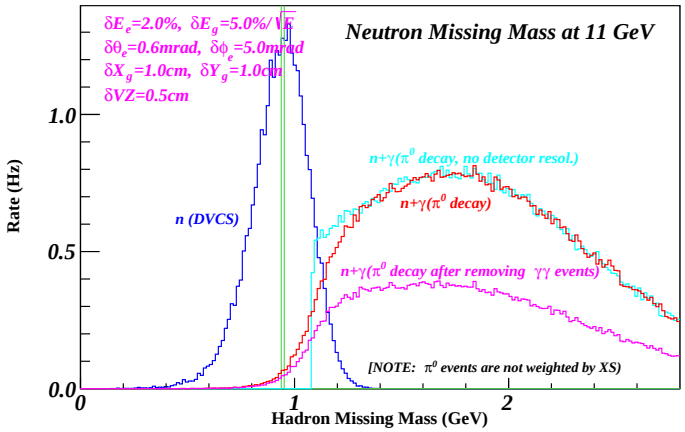

(b) E_{beam}=11 GeV

Figure 9: The neutron missing mass spectrum at E_{beam} = 8.8 and 11 GeV. The detector resolutions and the nucleon Fermi motion inside the nucleus were considered in the calculation. The π^0 background (red line) was normalized by roughly comparing with the preliminary result of the background study with recent 12 GeV Hall-A DVCS data. We also evaluate the π^0 combination (magenta line) after removing these events which we can detect by measuring both π^0 decayed photons. An updated version will be available once we have the $e^- n \to \pi^0$ exclusive cross section model.

7 Systematic Uncertainties

Sources	Relative Value
Beam Polarization	2%
Target Polarization	3%
Acceptance	3%
π^0 Contamination	$< 5\%$
Other Contamination	$< 5\%$
Radiation Correction	1%

Table 4: Expected systematic errors.

The detector related systematic errors are expected to be similar to the ones given in the E12-10-006 proposal as well as in other SIDIS experiments with SoLID, as shown in Table 4. The systematic error of the π^0 correction procedure and other background subtraction will be controlled at the 1%$\sim$5% level. We expect to provide a full list of systematic errors in the proposal.

8 Summary

We have presented a plan of using the SoLID to perform a precise measurement of the DVCS process with a longitudinally polarized electron beam at 8.8 and 11 GeV scattering off a transversely polarized ^{3}He target. We will extract three sets of asymmetries (BSA, TSA and DSA) as functions of Q^2, x_B, t and ϕ thanks to the high luminosity and large coverage features of the SoLID detectors. The full data sets with good statistics and well controlled systematic uncertainties will be used for the extraction of neutron GPDs, in particular the GPD E^n. Combined with the proton CFFs, the new data will be used to perform a flavor separation and extract the quark GPDs.

We have briefly described the experimental setup, presented the kinematic coverage and integrated rate of the DVCS events, as well as shown the projection of the asymmetries distributions by binning the simulation data. An overlook of the background situation was also given but required further study with a working model. We claimed that the experimental setup, which will also be used for several approved experiments, is straightforward and the modification of the existing configuration will be minimum to meet our requirement, although we have stronger demands on the detector resolutions. The SoLID collaboration has started to discuss the plan of the improvement and we will continue working on the actual proposal which will be submitted in the next PAC.

References

[1] D. Mller, D. Robaschik, B. Geyer, F.-M. Dittes and J. Hoeji, Fortsch. Phys. **42**, 101 (1994) [hep-ph/9812448].

[2] X. Ji, Phys. Rev. Lett. **78**, 610 (1997).

[3] X. -D. Ji, "Deeply virtual Compton scattering," Phys. Rev. D **55**, 7114 (1997) [hep-ph/9609381].

[4] A.V. Radyushkin, Phys. Rev. **D 56**, 5524 (1997).

[5] M. Diehl, Phys. Rep. **388**, 41 (2003).

[6] A. V. Belitsky and A. V. Radyushkin, "Unraveling hadron structure with generalized parton distributions," Phys. Rept. **418**, 1 (2005) [hep-ph/0504030].

[7] M. Guidal and M. Vanderhaeghen, "Generalized Parton Distributions in the valence region from Deeply Virtual Compton Scattering", [arXiv:1303.6600v3].

[8] Belitsky A V, Mueller D and Kirchner A 2002 Theory of deeply virtual Compton scattering on the nucleon *Nucl. Phys. B* **629** 323

[9] Approved Hall A experiment E12-06-114, "Measurements of Electron-Helicity Dependent Cross Sections of Deeply Virtual Compton Scattering with CEBAF at 12 GeV",
*http : //www.jlab.org/exp_prog/PACpage/PAC*38*/proposals/Previously_Approved/E*12 − 06 − 114*_Update.pdf*

[10] Approved CLAS12 experiment E12-06-119, "Deeply Virtual Compton Scattering with CLAS12 at 11 GeV",
*http : //www.jlab.org/exp_prog/PACpage/PAC*38*/proposals/Previously_Approved/E*12 − 06 − 119*_Update.pdf*

[11] Approved CLAS12 experiment E12-11-003, "Deeply Virtual Compton Scattering on the Neutron with CLAS12 at 11 GeV",
*http : //www.jlab.org/exp_prog/PACpage/PAC*38*/proposals/Previously_Approved/E*12 − 11 − 003*_Update.pdf*

[12] Vanderhaeghen M, Guichon P A M and Guidal M 1999 Deeply virtual electroproduction of photons and mesons on the nucleon: Leading order amplitudes and power corrections *Phys. Rev. D* **60** 094017

[13] E. Fuchey, A. Camsonne, C. Munoz Camacho, M. Mazouz, G. Gavalian, E. Kuchina, M. Amarian and K. A. Aniol *et al.*, "Exclusive Neutral Pion Electroproduction in the Deeply Virtual Regime," Phys. Rev. C **83**, 025201 (2011) [arXiv:1003.2938 [nucl-ex]].

[14] C. M. o. Camacho *et al.* [Jefferson Lab Hall A and Hall A DVCS Collaborations], "Scaling tests of the cross-section for deeply virtual compton scattering," Phys. Rev. Lett. **97**, 262002 (2006) [nucl-ex/0607029].

[15] F.X. Girod *et al.* [CLAS Collaborations], Deeply Virtual Compton Scattering Beam-Spin Asymmetries", Phys. Rev. Lett. **100**, 162002 (2008) [arXiv:0711.4805 [nucl-ex]].

[16] M. Mazouz *et al.* [Jefferson Lab Hall A Collaboration], "Deeply virtual compton scattering off the neutron," Phys. Rev. Lett. **99**, 242501 (2007) [arXiv:0709.0450 [nucl-ex]].

[17] Airapetian A *et al.* [HERMES Collaboration] 2001 Measurement of the beam spin azimuthal asymmetry associated with deeply-virtual Compton scattering *Phys. Rev. Lett.* **87**, 182001

[18] Airapetian A *et al.* [HERMES Collaboration] 2012 Beam-helicity and beam-charge asymmetries associated with deeply virtual Compton scattering on the unpolarised proton *JHEP* **1207**, 032

[19] Airapetian A *et al.* [HERMES Collaboration] 2010 Exclusive Leptoproduction of Real Photons on a Longitudinally Polarised Hydrogen Target *JHEP* **1006**, 019

[20] Airapetian A *et al.* [HERMES Collaboration] 2008 Measurement of Azimuthal Asymmetries With Respect To Both Beam Charge and Transverse Target Polarization in Exclusive Electroproduction of Real Photons *JHEP* **0806**, 066

[21] Airapetian A *et al.* [HERMES Collaboration] 2011 Measurement of double-spin asymmetries associated with deeply virtual Compton scattering on a transversely polarized hydrogen target *Phys. Lett. B* **704**, 15

[22] Airapetian A *et al.* [HERMES Collaboration] 2007 The beam-charge azimuthal asymmetry and deeply virtual Compton scattering *Phys. Rev. D* **75**, 011103

[23] Airapetian A *et al.* [HERMES Collaboration] 2009 Separation of contributions from deeply virtual Compton scattering and its interference with the Bethe-Heitler process in measurements on a hydrogen target *JHEP* **0911**, 083

[24] Airapetian A *et al.* [HERMES Collaboration] 2010 Nuclear-mass dependence of azimuthal beam-helicity and beam-charge asymmetries in deeply virtual Compton scattering *Phys. Rev. C* **81**, 035202

[25] SoLID Collaboration, "Solenoial Large Intensity Device Preliminary Conceptual Design Report," $http://hallaweb.jlab.org/12GeV/SoLID/files/solid\_precdr.pdf$

[26] "Target Single Spin Asymmetry in Semi-Inclusive Deep-Inelastic (e,e'$\pi^{\pm}$) Reaction on a Transversely Polarized ^3He Target at 11 GeV", $http://hallaweb.jlab.org/collab/PAC/PAC34/PR-09-014-transversity.pdf$

[27] M. Defurne *et al.* [Hall A Collaboration], arXiv:1504.05453 [nucl-ex].

[28] H. S. Jo *et al.* [CLAS Collaboration], arXiv:1504.02009 [hep-ex].